J. of Thermal Science Vol.6, No.3

JTS

Forced Convective Heat Transfer in a Porous Plate Channel

Peixue Jiang Zhan Wang Zepei Ren Buxuan Wang

Department of Thermal Engineering, Tsinghua University, Beijing 100084, China

Forced convective heat transfer in a plate channel filled with metallic spherical particles was investigated experimentally and numerically. The test section, 58 mm×80 mm×5 mm in size, was heated by a 0.4 mm thick plate electrical heater. The coolant water flow rate ranged from 0.015 to 0.833 kg/s. The local wall temperature distribution was measured along with the inlet and outlet fluid temperatures and pressures. The results illustrate the heat transfer augmentation and increased pressure drop caused by the porous medium. The heat transfer coefficient was increased 5-12 times by the porous media although the hydraulic resistance was increased even more. The Nusselt number and the heat transfer coefficient increased with decreasing particle diameter, while the pressure drop decreased as the particle diameter increased. It was found that, for the conditions studied (metallic packed bed), the effect of thermal dispersion did not need to be considered in the physical model, as opposed to a non-metallic packed bed, where thermal dispersion is important.

Keywords: convective heat transfer, porous media, plate channel, heat transfer enhancement, pressure drop.

INTRODUCTION

Heat transfer enhancement techniques play a very important role in thermal control technologies used with microelectronic chips, powerful laser mirrors, aerospace craft, thermal nuclear fusion, etc. It is widely recognized that the heat transfer can be increased by increasing the surface area in contact with the coolant. Tuckerman and Pease[1,2] pointed out that for laminar flow in confined channels, the heat transfer coefficient is inversely proportional to the width of the channel since the limiting Nusselt number is constant. They built a water-cooled integral heat sink with microscopic flow channels, typically 50 μm wide and 300 μm wide and 300 μm deep, and demonstrated that extremely high power density circuits could be cooled with a surface flux of 790 W/cm^2 or even more. Mahalingam[3] confirmed the superiority of microchannel cooling on a silicon substrata with a surface area of 5 cm × 5 cm using water and air as coolants. In recent years many researchers have studied the heat transfer augmentation produced by microchannels.

Porous structures are another effective heat transfer augmentation technique. Porous structures intensify the mixing of the flowing fluid and enhance the convective heat transfer. Several cooling systems using porous structures have been applied to cooling mirrors in powerful lasers[4,5] and cooling phased-array radar systems[6]. Very high heat fluxes (4×10^7 W/m^2) can be obtained using single-phase water flow[5]. Chrysler and Simons[7] suggested the use of packed beds of spherical particles to enhance convective heat transfer from microelectronic chips while Kuo and Tien[8] suggested the use of foam metal for the same application. Jeigarnik et al.[9] and Haritonov et al.[4] numerically and experimentally investigated the convective heat transfer on flat plates and in channels filled with porous material. The porous media increased the heat transfer coefficient 5–10 times although the hydraulic resistance was increased even more. Hwang and Chao[10] experimentally and numerically studied convective heat transfer in sintered porous channels.

Received March, 1997.

Nasr et al.[11] experimentally studied the forced convection heat transfer from a circular cylinder embedded in a packed bed of spherical particles showing that the packed bed greatly increased the Nusselt number (up to seven times for aluminum spheres).

The influence, such as non-Darcian effects, variable porosity, variable properties, and thermal dispersion in the porous medium on the fluid flow and heat transfer has been widely studied[12-20]. A comprehensive review of heat and fluid flow characteristics in packed beds was published by Achenbach[21], but there are some problems that still need to be investigated further. For example, heat transfer increases as the particle diameter increases according to [13-15, 18-19], but Jeigarnik et al.[9], Hwang and Chao[10] and Nasr et al.[11] found the opposite result. The experiments of Jeigarnik et al.[9] used water and Hwang and Chao[10] and Nasr et al.[11] used air flowing through a packed bed made of comparatively high thermal-conductivity particles; so, the heat transfer coefficients on the wall were controlled mainly by heat conduction from the solid particles to the wall. When the particle diameter was decreased, the contact surface between fluid and particles increased, so the heat transfer coefficient increased. This has been analyzed by Jiang et al.[20]. However, it needs to be verified experimentally.

The present paper reports the results of an experimental study and corresponding numerical simulation of forced convective heat transfer in a plate channel filled with metallic spherical particles. The numerical results are compared with experimental data. The effect of thermal dispersion, particle diameter and particle conductivity on convective heat transfer in metallic packed bed is analyzed.

EXPERIMENTAL APPARATUS AND DATA REDUCTION

The geometry is depicted schematically in Fig.1. The size of the test section was 58 mm × 80 mm ×5 mm. The upper plate of the channel received a constant heat flux, q_{1w}, while the bottom and the side plates were adiabatic. The flow entered the channel with an average velocity u_o and constant temperature T_{of}. Adiabatic sections (1 mm long) were placed before and after the heated section. The coolant water flow rate ranged from 0.015 to 0.833 kg/s.

In electronic cooling, micro-electronic devices may be damaged by local excessive high temperatures of the heat sink as opposed to the average temperatures, so the local wall temperature distribution was measured so as to determine the local heat transfer coefficient. The Nusselt numbers along the plate channel with porous media are then compared to those without porous media.

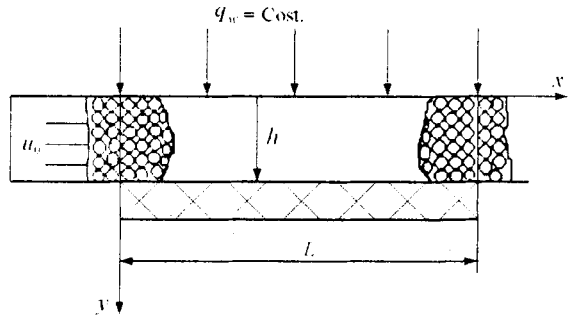

Fig.1 Schematic diagram of the physical system

The experimental apparatus, shown schematically in Fig.2, consisted of a water tank, a pump, a test section, a heat exchanger, and instrumentation to measure temperatures and pressures and electrical power inputs. The test section was made of 2 mm thick stainless steel plate and thermally insulated from the outside environment. There were 1 mm unheated porous sections before and after the heated section. The plate channel was filled with packed metallic (stainless steel or iron) particles. The average bead diameters were 0.428 mm for stainless steel particles and 0.85 mm for iron particles. Special care was taken in packing the beads to ensure uniformity in the structure of the porous medium. The spheres were poured randomly

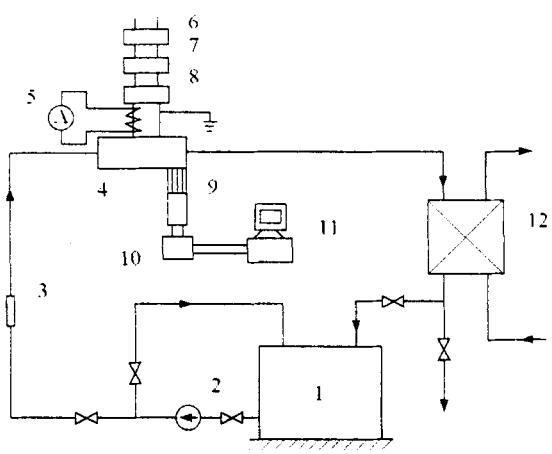

1. water tank; 2. pump; 3. filter; 4. test section;
5. current meter; 6. voltage stabilizer; 7. voltage regulator; 8. transformer; 9. multiplexer;
10. digital multimeter; 11. personal computer,
12. plate heat exchanger

Fig.2 Experimental apparatus

into the channel, leveled and then shaken. This procedure was repeated until no more beads could be placed into the channel. The spheres were supported by two perforated plates and fine mesh stainless steel screens at the inlet and outlet of the test section. The measured global porosity for the entire packed channel was 0.365 for d_p=0.428 mm and 0.381 for d_p=0.85 mm.

The upper plate was heated by a 0.4 mm thick plate heater using low voltage alternating current to simulate a heat sink with constant heat flux. A mica sheet was placed between the heater and the stainless steel plate channel surface. The small air gap between the mica sheet and the stainless steel plate channel surface was filled by a high thermal conductivity paste to minimize the contact resistance. The heater voltage and current were measured by digital multimeters. The electric power input to the heater was calculated from the measured current and voltage readings.

The local temperature of the plate channel was measured with 22 copper-constantan thermocouples at the locations shown in Fig.3. Ten thermocouples were attached to the upper plate channel surface (0.5 mm below the surface) along the centerline and ten thermocouples were attached to the inner plate channel surface (1 mm deep) along the centerline at the same axial locations as those on upper surface. Two more thermocouples were attached to the upper

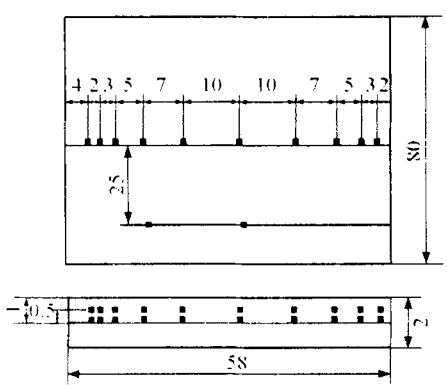

Fig.3 Thermocouple locations (the dots represent thermocouples; the distances are in mm)

plate channel surface along a line 2.5 cm away from the centerline to monitor the temperature variations at the cross sections. The thermocouple leads first ran along cross-sectional grooves and then along the longitudinal grooves toward the channel end. The groove were covered with soft metal and then smoothed. The inlet water temperature was measured by a thermocouple located at the inlet, approximately 4.5 cm upstream from the heated section. Three thermocouples were located at the outlet of the plate channel, approximately 4.5 cm downstream from the heated section and 1 thermocouple was located in the tube 17.5 cm downstream from the heated section to measure the bulk temperature at the exit. Prior to installation, the thermocouples were calibrated using a constant temperature oil bath. The overall accuracy was found to be well within ±0.2C. The pressures at the inlet and outlet were measured using accurate manometers with an accuracy of 0.25% of the full scale range of 1.6 MPa. The measured temperatures and pressures were used to determine the values of the thermophysical properties needed for the calculations. The flow rate was measured by weighting the fluid exiting the channel for a given time period. A regulating valve in the line allowed the flow rate in the test section to be varied from approximately 0.015 to 0.833 kg/s.

Water was chosen as the working fluid because of its availability and wide application. For each test, the flow rate, input power and inlet fluid temperature were fixed. The temperatures were measured with 27 thermocouples connected through a multiplexer to a digital multimeter (HP34401A) and a personal computer. The temperatures were monitored and recorded after steady-state conditions were reached. The flow rate, inlet and outlet fluid bulk temperatures, and electric power input were also recorded. The local bulk mean temperature of the fluid at the measuring section was calculated from the inlet temperature, flow rate and power input, or from the inlet and outlet temperatures using linear interpolation. The fluid enthalpy rise was checked against the electric power input. The experimental errors in the heat balance were less than 5%.

The bulk porosity of the porous medium (packed bed) was computed for each run according to the following definition:

$$\varepsilon = \frac{V_t - V_p}{V_t} \tag{1}$$

Where V_p is the ratio of the measured weight of the particles that occupy the test section to the density and V_t is the total porous channel volume.

Preliminary tests were performed for data calibration and error estimation. The errors in the temperature measurements were due to inaccuracies in the initial calibration of the thermocouple and the recorder readings. The maximum error was within ±0.2 °C for the temperature measurement. The maximum errors both in the flow rate and pressure drop across the test section were less than 5 percent.

The local heat transfer coefficient, h_x, and Nusselt number, $\mathrm{Nu_X}$, at each axial location were calculated as

$$h_x = q_x/(T_{wx} - T_{fb}) \tag{2}$$

$$\mathrm{Nu_X} = h_x D_e/k_f \tag{3}$$

The mean heat transfer coefficient, h_m, and mean Nusselt number, Num, in the plate channel were calculated as

$$h_m = q_w/(T_{wm} - T_{fm}) \tag{4}$$

$$\mathrm{Num} = h_m D_e/k_m \tag{5}$$

where $q_w = Q/A_{\mathrm{heated}}$ is the heat input per unit area, Q is the power input, A_{heated} is the area of the heated test section; $D_e = 2HW/(H+W)$ is the hydraulic diameter, H and W are the channel height and width, respectively; k_f is the thermal conductivity of the fluid evaluated at the local film temperature, $T_{\mathrm{film}} = (T_{fb} + T_{wx})/2$, T_{wx} is the local temperature of the heat transfer surface calculated using the measured temperatures of the wall, T_{fb} is the local bulk temperature of the fluid, T_{wm} is the mean temperature of the heat transfer surface, T_{fm} is the mean temperature of the fluid in the plate channel, and k_m is the thermal conductivity of the fluid evaluated at the mean temperature T_{fm}.

The pressure drop was calculated as

$$\Delta P = P_{in} - P_{out} \tag{6}$$

Where P_{in} and P_{out} are the pressures at the inlet and outlet of the test section, respectively.

The Reynolds number was defined as

$$Re_D = uD_e/\nu_m \tag{7}$$

where u is the velocity of the fluid at the inlet and ν_m is the kinematic viscosity of the fluid evaluated at the mean fluid temperature.

Steady-state was said to be reached when the deviations of the wall temperatures and the inlet and outlet temperatures were all within ± 0.2°C for 10 min. The experimental uncertainties in the Nusselt number, mainly due to experimental errors in the heat balance, temperature measurements and temperature calculations of the heat transfer surface, were estimated to be $\pm 20\%$.

The experimental setup was evaluated by comparing the results obtained for convective heat transfer in a bare plate channel with established correlations as proposed by Petukhov et al.[22] for turbulent flow and by Gnielinski[23] for transition flow. Fig.4 shows the experimental results compared with the correlations for various Reynolds numbers. The average difference is $\pm 11\%$, while the maximum difference is $\pm 24\%$.

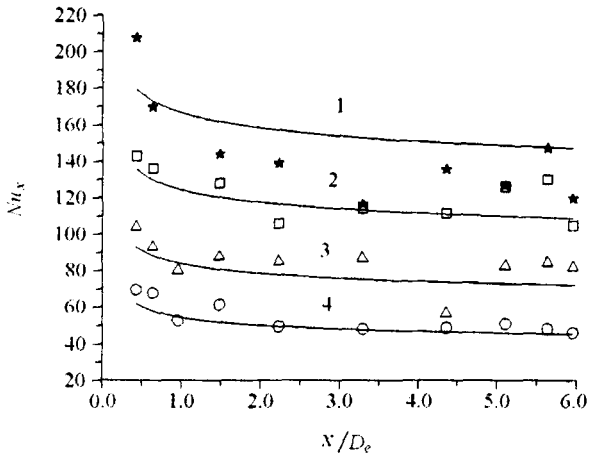

1. ★ $Re_D = 1.67 \times 10^4$, $q_w = 1.16 \times 10^5$ W/m^2;
2. □ $Re_D = 1.16 \times 10^4$, $q_w = 1.16 \times 10^5$ W/m^2;
3. △ $Re_D = 7493$, $q_w = 1.14 \times 10^5$ W/m^2;
4. ⊙ $Re_D = 4736$, $q_w = 1.14 \times 10^5$ W/m^2

★, □, △, ⊙ experimental data;
——— predicted values

Fig.4 Comparison of measurements with predictions for bare plate channel

MATHEMATICAL FORMULATION AND NUMERICAL METHOD

The physical model and the coordinate system are shown in Fig.1. The model considers fluid flow and convective heat transfer in a plate channel filled with homogeneous, isotropic solid particles. The fluid is single-phase and the flow is two-dimensional, steady, non-Darcian flow. Because only high Peclet number flow is treated, longitudinal conduction in the fluid and the pressure variation in y direction are negligibly small.

The steady-state, two-dimensional governing equations for single-phase fluid flow in an isotropic, homogeneous porous medium based on the Brinkman-Darcy-Forchheimer model and the thermal equilibrium assumption with consideration of variable thermophysical properties, variable porosity and thermal dispersion can be written in the following form[20]:

$$\frac{\partial(\rho_f \varepsilon u_p)}{\partial x} + \frac{\partial(\rho_f \varepsilon v_p)}{\partial y} = 0 \tag{8}$$

$$\frac{\partial(\rho_f \varepsilon u_p u_p)}{\partial x} + \frac{\partial(\rho_f \varepsilon v_p u_p)}{\partial y} = -\frac{\partial(\varepsilon p)}{\partial x}$$

$$-\varepsilon^2 \frac{\mu_f}{K} u_p - \varepsilon^3 \frac{\rho_f F}{\sqrt{K}} |U_p| u_p + \frac{\partial}{\partial y}\left(\varepsilon \mu_e \frac{\partial u_p}{\partial y}\right) \tag{9}$$

$$\frac{\partial(\rho_f \varepsilon u_p h_f)}{\partial x} + \frac{\partial(\rho_f \varepsilon v_p h_f)}{\partial y} = \frac{\partial}{\partial y}\left[\frac{(\lambda_m + \lambda_d)}{c_{pf}} \frac{\partial h_f}{\partial y}\right] \tag{10}$$

$$\int_0^h \rho_f \varepsilon u_p dy = \rho_0 u_0 h \tag{11}$$

The corresponding boundary conditions are:

$$x = 0, u_p = u_p(y), v_p = v_p(y), T_f = T_{f0}$$
$$y = 0, u_p = v_p = 0, q_{1w} = -\lambda_m \partial T/\partial y$$
$$y = h, u_p = v_p = 0, q_{2w} = 0$$

Parameters used in Eqs.(8)-(11) were obtained from Jiang et al.[18], Cheng et al.[24] and Zehner and Schlunder[25]:

$$K = d_p^2 \varepsilon^3/(150(1-\varepsilon)^2); \quad F = 1.75/(\sqrt{150}\varepsilon^{3/2});$$

$$\lambda_d = 0.025(\rho c_p)_f d_p |U_p|(1-\varepsilon);$$

$$\varepsilon = \varepsilon_\infty(1 + e^{-6y/d_p}) \quad (0 \le y \le h/2);$$

$$\varepsilon = \varepsilon_\infty(1 + e^{-6(h-y/d_p}) \quad (h/2 \le y \le h)$$

$$\frac{\lambda_m}{\lambda_f} = \left[1 - \sqrt{1-\varepsilon}\right] + \frac{2\sqrt{1-\varepsilon}}{1-\sigma B}$$

$$\left[\frac{(1-\sigma)B}{(1-\sigma B)^2} \ln\left(\frac{1}{\sigma B}\right) - \frac{B+1}{2} - \frac{B-1}{1-\sigma B}\right]$$

$$B = 125((1-\varepsilon)/\varepsilon)^{10/9}; \quad \sigma = \lambda_f/\lambda_s;$$

In the momentum equation, Eq.(9), the terms on the left-hand side are the inertia terms. The terms on the right-hand side are the pressure gradient term, the Darcy term, the Forchheimer term and the Brinkman term, respectively. When $\varepsilon = 1, k$ is infinity and the momentum equation describes Newtonian fluid in a parallel plate channel without porous media. Therefore, Eq.(9) is suitable for $0 < \varepsilon \le 1$. The thermophysical properties of water were obtained from Rivkin and Aleksandrov[26] in tabular form. The property values used in the calculations were determined by second-order interpolation relative to enthalpy.

The governing equations were solved numerically using the finite difference method. With the appropriate dimensionless parameters, the governing equations, Eqs.(8)-(11), and the boundary conditions were first transformed into dimensionless form. Then, the dimensionless governing equations were discretized using control volume integration. The solution for Eqs.(8)-(11) can march in the downstream direction, Jiang et al.[20]. Due to the no-slip boundary conditions and variable porosity, steep velocity gradients were expected near the wall. Therefore, a non-uniform grid was employed with 52 grid points normal to the wall and 202 grid points in the axial direction.

The desired convective heat transfer parameters were evaluated using Eqs.(2)-(5). The pressure drop was calculated as

$$\Delta p = \left|\rho_o u_o^2 \sum_{j=2}^{N} \left[\left(\frac{dp^+}{dx^+}\right)_j (\Delta x^+)_f\right]\right| \tag{12}$$

RESULTS AND DISCUSSION

Local Wall Temperature

In micro-electronics and powerful lasers, devices can be damaged by local high temperatures; therefore, the temperature distribution along the flow direction of the test section is of practical interest in design. Also, the local wall temperatures are needed to calculate the local heat transfer coefficient. Fig.5 and Fig.6 present the local wall temperature distribution (measured 1 mm below the surface) as a function of Reynolds number for d_p = 0.355 ~0.5 mm and d_p = 0.80 ~0.9 mm, respectively. The local wall temperature increases in the axial direction and increases with decreasing Reynolds number.

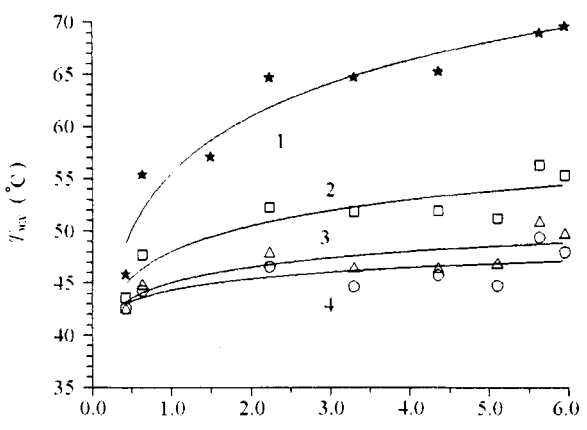

1. ★ Re_D = 355.9, q_w = 1.13 × 10^5 W/m^2;
2. □ Re_D = 924.9, q_w = 1.14 × 10^5 W/m^2;
3. △ Re_D = 2445.3, q_w = 1.12 × 10^5 W/m^2;
4. ⊙ Re_D = 3967.8, q_w = 1.14 × 10^5 W/m^2

Fig.5 Wall temperature distribution for porous plate channel (d_p = 0.355 ~ 0.5 mm, stainless steel particles)

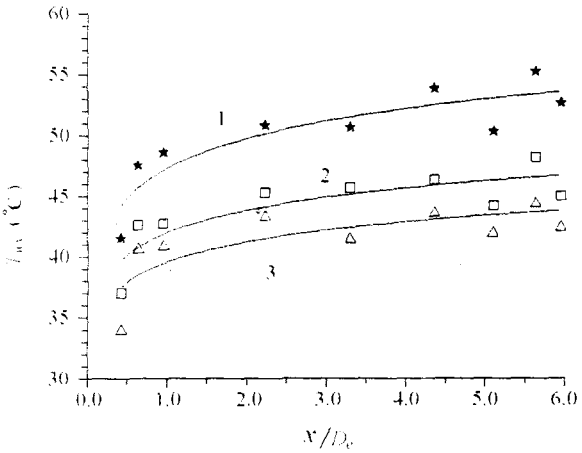

1. ★ $Re_D = 940.2$, $q_w = 1.12 \times 10^5$ W/m^2;
2. □ $Re_D = 2857.7$, $q_w = 1.13 \times 10^5$ W/m^2;
3. △ $Re_D = 3614.0$, $q_w = 1.18 \times 10^5$ W/m^2;

Fig.6 Wall temperature distribution for porous plate channel ($d_p = 0.8 \sim 0.9$ mm, cast iron particles)

HEAT TRANSFER ENHANCEMENT DUE TO THE PARTICLES

Fig.7 and Fig.8 show the distribution of the local Nusselt number for different Reynolds numbers for

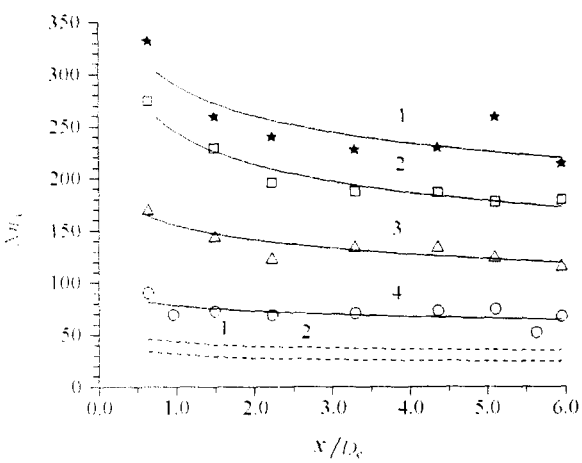

1. ★ $Re_D = 3967.8$, $q_w = 1.14 \times 10^5$ W/m^2;
2. □ $Re_D = 3083.0$, $q_w = 1.15 \times 10^5$ W/m^2;
3. △ $Re_D = 924.9$, $q_w = 1.14 \times 10^5$ W/m^2;
4. ⊙ $Re_D = 355.9$, $q_w = 1.13 \times 10^5$ W/m^2

★, □, △, ⊙ experimental data for porous plate channel;

– – – – – calculated values for bare plate channel

Fig.7 Comparison of measured local Nusselt numbers for porous plate channel with bare plate channel predictions ($d_p = 0.355 \sim 0.5$ mm, stainless steel particles)

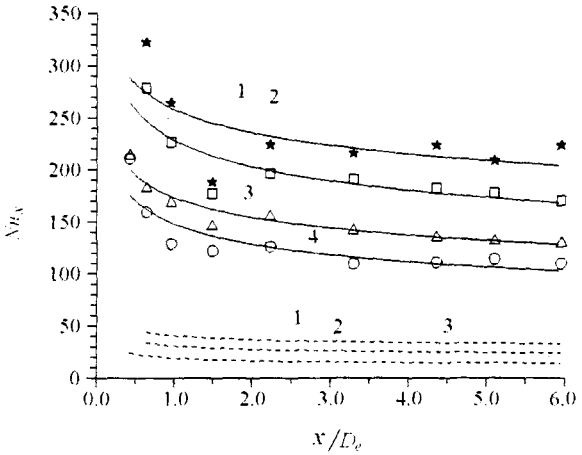

1. ★ $Re_D = 3614.0$, $q_w = 1.18 \times 10^5$ W/m^2;
2. □ $Re_D = 2857.7$, $q_w = 1.13 \times 10^5$ W/m^2;
3. △ $Re_D = 2003.7$, $q_w = 1.13 \times 10^5$ W/m^2;
4. ⊙ $Re_D = 9402$, $q_w = 1.12 \times 10^5$ W/m^2

★, □, △, ⊙ experimental data for porous plate channel;

– – – – – calculated values for bare plate channel

Fig.8 Comparison of measured local Nusselt numbers for porous plate channel with bare plate channel predictions ($d_p = 0.8 \sim 0.9$ mm, cast iron particles)

$d_p = 0.355 \sim 0.5$ mm and $d_p = 0.80 \sim 0.9$ mm, respectively. The local Nusselt number is increasing as the Reynolds number increases. Large local convective heat transfer coefficients can be obtained for relatively low Reynolds numbers. To illustrate to how to transfer along the plate channel, the results are compared with the empty plate channel in Fig.7 and Fig.8 for the local Nusselt number and in Fig.9 for the mean Nusselt number. The packed bed greatly increases the Nusselt number (up to 12 times), indicating that the particles can be used as an effective method to enhance forced convective heat transfer. In addition, under the conditions studied here, lowering the Reynolds number increases the amount of enhancement. It can also be seen from Fig.9 that the Nusselt number and the heat transfer coefficient increase with decreasing particle diameter (note that the thermal conductivity of the cast iron particles with $d_p = 0.80 \sim 0.9$ mm is larger than that of the stainless steel particles with $d_p = 0.355 \sim 0.5$ mm), which corresponds to the experimental results of Jeigarnik et al.[9] and Nasr et al.[11].

Heat Transfer Coefficient and Effect of Thermal Dispersion

The numerical results were checked in numerous ways to verify the reliability of the physical-

mathematical model. The solution procedures and the numerical simulation program are described by Jiang et al.[20]. Because the thermophysical properties of water are nearly independent of pressures, the values of the thermophysical properties of water at $p = 0.5$ MPa were used in numerical calculations. The other conditions for the numerical solutions were: $M = 0.0154 \sim 0.194$ kg/s; $q_{1w} \approx 10^5$ W/m^2; $d_p = 0.428$ mm, $\varepsilon = 0.365$, $k_s = 16$ W/(mK) (for stainless steel particles); $d_p = 0.85$, $\varepsilon = 0.381$, $k_s = 30$ W/(mK) (for cast iron particles); $L = 58$ mm; $h = 5$ mm.

A comparison of the numerically predicted and experimentally determined local convective heat transfer coefficients in the porous plate channel is presented in Fig.10 for stainless steel particles and in Fig.11 for cast iron particles. Fig.9 shows a comparison of mean convective heat transfer coefficients. Figs.10-11 show that when thermal dispersion is not considered, the predicted heat transfer coefficients and Nusselt numbers agree well with the experimental results. If thermal dispersion is considered with $c = 0.025$, the predicted heat transfer coefficients are much higher than the experimental results. These results differ from the case for non-metallic porous media as discussed by Jiang et al.[18,19], where the thermal dispersion effect must be considered. The largest difference between the metallic porous media and non-metallic porous media is the different thermal conductivities of the packed beds. For non-metallic packed beds, the stagnant effective thermal conductivity of the fluid and porous media

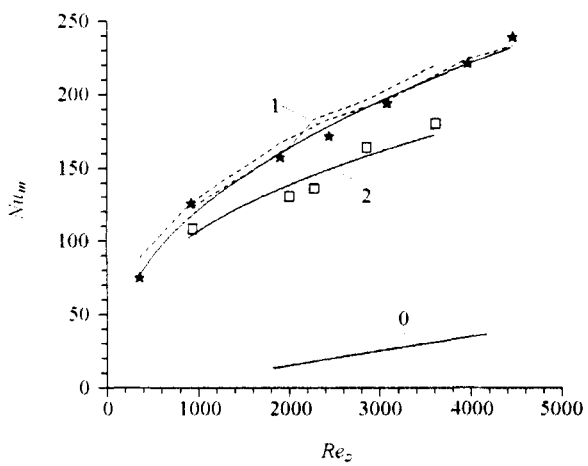

1. ★ $d_p = 0.355 \sim 0.5$, 2. □ $d_p = 0.8 \sim 0.9$ mm,
★, □ experimental data for porous plate channel;
– – – – – numerical simulation results ($\lambda_d = 0$);
0 calculated values for bare plate channel

Fig.9 Comparison of measured mean Nusselt numbers for porous plate channel with bare plate channel correlations

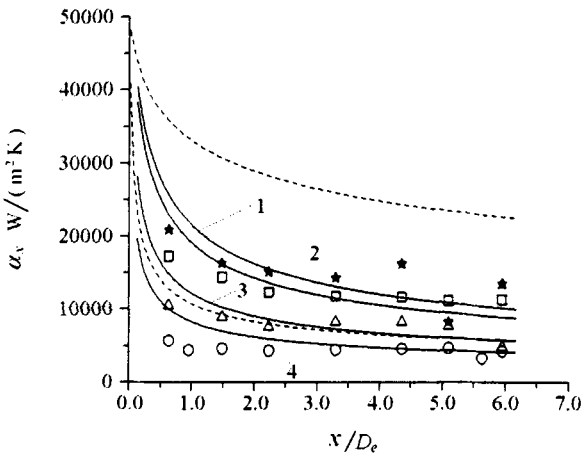

1. ★ $Re_D = 3967.8$, $q_w = 1.14 \times 10^5$ W/m^2;
2. □ $Re_D = 3083.0$, $q_w = 1.15 \times 10^5$ W/m^2;
3. △ $Re_D = 924.9$, $q_w = 1.14 \times 10^5$ W/m^2;
4. ⊙ $Re_D = 355.9$, $q_w = 1.13 \times 10^5$ W/m^2
★, □, △, ⊙ experimental data for porous plate channel;
———— numerical simulation results (λ_d=0);
– – – – – numerical simulation results ($\lambda_d \neq 0$)

Fig.10 Comparison of measured and numerically simulated local heat transfer coefficient for porous plate channel ($d_p = 0.428$ mm)

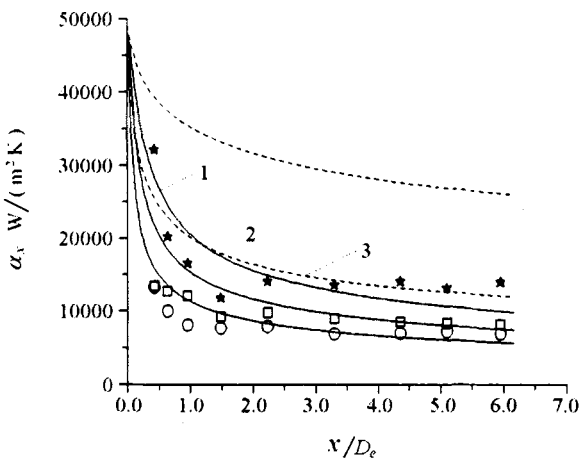

1. ★ $Re_D = 3614.0$, $q_w = 1.18 \times 10^5$ W/m^2;
2. □ $Re_D = 2857.7$, $q_w = 1.13 \times 10^5$ W/m^2;
4. ⊙ $Re_D = 9402$, $q_w = 1.12 \times 10^5$ W/m^2
★, □, ⊙ experimental data for porous plate channel;
———— numerical simulation results (λ_d=0);
– – – – – numerical simulation results ($\lambda_d \neq 0$)

Fig.11 Comparison of measured and numerically simulated local heat transfer coefficient for porous plate channel ($d_p = 0.85$ mm)

system calculated using the formula given in Section 3 for λ_m is nearly the same as the thermal conductivity of the fluid, λ_f. Since the thermal dispersion increases the convective heat transfer, the additional

thermal conductivity resulting from the thermal dispersion must be included. But for metallic packed beds, the stagnant effective thermal conductivity of the fluid and porous media system calculated using the formula given in Section 3 for λ_m is much higher than the fluid thermal conductivity λ_f. Therefore, including the additional thermal conductivity resulting from thermal dispersion λ_d for metallic packed beds overestimates the total convective heat transfer. This conclusion is in agreement with Nasr et al.[11]. The thermal dispersion model needs further improvement by comparing the numerical simulation results with experimental data using a wide-range of porous media materials. The constant c in the formula for the stagnant effective thermal conductivity of the fluid and porous media system may be not constant for all porous media materials. The non-thermal equilibrium model also needs further improvement to be applicable to numerical simulation of convective heat transfer in metallic packed beds. Research on these two topics is currently in progress.

Effect of Particle Thermal conductivity and Particle Diameter on Heat Transfer

Fig.12 and Fig.13 illustrate the numerical simulation results showing the effect of particle diameter and particle conductivity on heat transfer coefficient. Increasing the thermal conductivity of the particles causes the convective heat transfer coefficient to increase. The experimental data shows that the heat transfer coefficient increases with decreasing metallic particle diameter as shown in Fig.9. But the numerical simulation based on the thermal equilibrium assumption and without consideration of thermal dispersion, Eqs.(8)-(11), for metallic porous media can not accurately model the effect of particle diameter on heat transfer as shown in Fig.9 and Fig.13. Therefore, the well-established physico-mathematical model for non-metallic porous media, Eqs.(8)-(11), may be not completely suitable for metallic packed beds. A numerical model including the non-thermal equilibrium model for metallic porous media (with high thermal conductivity) needs to be developed.

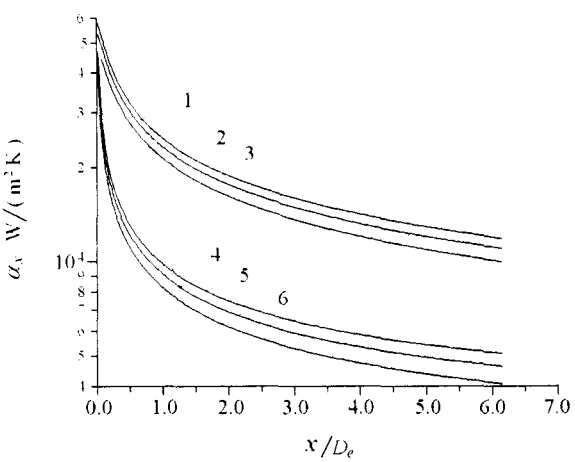

Fig.12 Numerical simulation results for different solid particle thermal conductivities
(d_p = 0.428 mm, ε = 0.365)
1,2,3 M = 0.1764 kg/s;
4,5,6 M = 0.0154 kg/s;
1,4 λ_s = 50 W/(mK);
2,5 λ_s = 30 W/(mK);
3,6 λ_s=16 W/(mK)

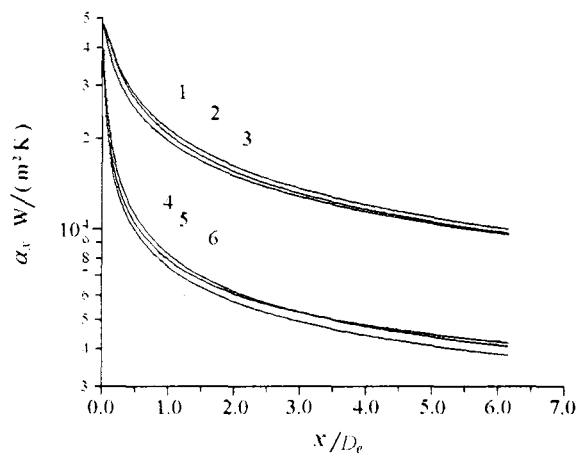

Fig.13 Numerical simulation results for different solid particle diameters
(λ_s = 16 W/(mK), ε = 0.365)
1,2,3 M = 0.1764 kg/s; 4,5,6 M = 0.0154 kg/s;
1,4 d_p = 0.08 mm; 2,5 d_p = 0.428 mm;
3,6 d_p=0.85 mm

Pressure Drop and Friction Factor

Fig.14 shows the pressure drop in the porous plate

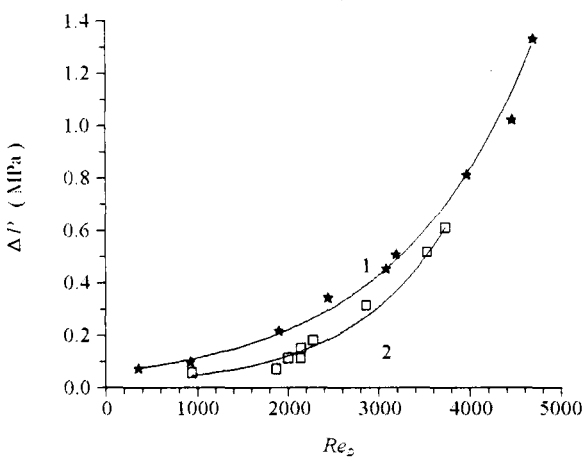

Fig.14 Measured pressure drop as a function of Reynolds number
1, ★ $d_p = 0.355 \sim 0.5$,
2, □ $d_p = 0.8 \sim 0.9$ mm

channel as a function of Reynolds number. The pressure drop was greatly increased by the packed bed and increases as the particle diameter decreases. Fig.15 compares the friction factor, f_e, predicted by the numerical simulation, the experimental data and the friction factor equation given by Aerov and Tojec[27]:

$$f_e = \frac{\varepsilon^3}{1-\varepsilon}\frac{\rho_f d_p}{3G^2}\frac{\Delta p}{L} = \frac{36.4}{Re_e} + 0.45 \quad (\text{for} \quad Re_e < 2000) \tag{13}$$

where $G = \rho u$ is the mass flux per unit area and $Re_e = 2Gd_p/(3\mu_f(1-\varepsilon))$ is the equivalent Reynolds number. The numerically calculated values of f_e agree well with the experimental data for stainless steel particles ($d_p = 0.355 \sim 0.5$ mm) and the values predicted using Eq.(13).

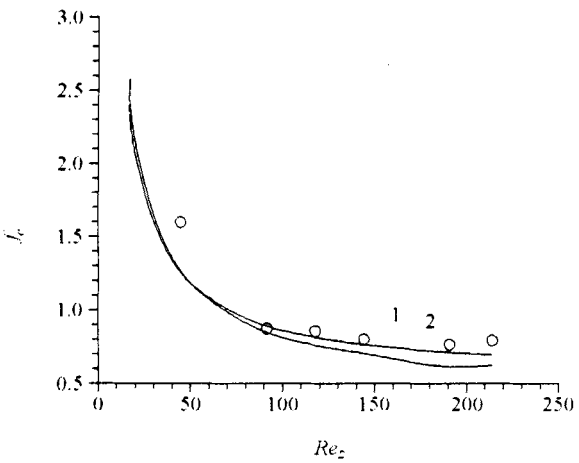

Fig.15 Friction factor in porous plate channel
1 numerical simulation;
2 calculation using Eq.(13);
⊙ experimental results ($d_p = 0.428$ mm)

CONCLUSION

Forced convective heat transfer in a plate channel filled with metallic spherical particles was investigated experimentally and numerically. The main results can be summarized as:

(1) The packed bed greatly increases the Nusselt number (up to 12 times), showing that the packed metallic particles are an effective method for enhancing forced convective heat transfer. Smaller metallic particle diameters and higher particle thermal conductivities result in larger convective heat transfer coefficients. In addition, for the conditions studied here, lower Reynolds numbers increased the degree of enhancement.

(2) For metallic packed beds, the effect of thermal dispersion need not be considered in the numeric model. Including the additional thermal conductivity resulting from thermal dispersion λ_d for metallic packed beds overestimates the convective heat transfer. This conclusion differs from the model for non-metallic packed beds.

(3) The pressure drop was greatly increased by the packed bed. The pressure drop increased as the particle diameter decreased. The friction factor, f_e, can be calculated using Eq.(13) and by the numeric simulation.

Acknowledgment

The project was financially supported by funds from the National Natural Science Foundation of China (No.59506004), the China State Education Committee Fund for Excellent Young Teachers and the Natural Science Fundamental Research Foundation of Tsinghua University, Beijing, China.

REFERENCES

[1] D.B. Tucherman and R.F. Pease, "High-Performance Heat Sinking for VLSI," Electron Device Lett., **2,** pp.126-129, (1981).

[2] D.B. Tuckerman and R.F. Pease, "Ultra High Thermal Conductance Microstructures for Cooling Integrated Circuits," IEEE CH781-4, pp.145-149, (1982).

[3] M. Mahalingam, "Thermal Management in Semiconductor Device Packaging," Proc. IEEE, **73,** pp.1396-1404, (1985).

[4] V.V. Haritonov, U.N. Kiceleva, V.V., Atamanov, U.A. Jeigarnik and F.P. Ivanov, "Generalization of the Results on Heat Transfer Intensification in Channels with Porous Insertion," (in Russian), *Teplofizika Vys. Temp.*, **32,** No.3, pp.433-440, (1994).

[5] V.I. Subbojin and V.V. Haritonov, "Thermophysics of Cooled Laser Mirror," (in Russian), *Teplofizika Vys. Temp.*, **29,** No.2, pp.365-275, (1991).

[6] J.L. Lage, A.K. Weinert, D.C. Price and R.M. Weber, "Numerical Study of a Low Permeability Microporous Heat Sink for Cooling Phased-Array Radar Systems," *Int. J. Heat Mass Transfer,* **39,** No.17, pp.3633-3647, (1996).

[7] G.M. Chrysler and R.E. Simons, "An Experimental Investigation of the Forced Convection Heat Transfer Characteristics of Fluorocarbon Liquid Flowing Through a Packed-Bed for Immersion Cooling of Microelectronic Heat Sources," in AIAA/ASME Thermophysics and Heat Transfer Conference, Cryogenic and Immersion Cooling of Optics and Electronic Equipment, ASME HTD-**131,** pp.21-27, (1990).

[8] S.M. Kuo and C.L. Tien, "Heat Transfer Augmentation in a Foam-Material Filled Duct with Discrete Heat

Sources," in Intersociety Conference on Thermal Phenomena in the Fabrication and Operation of Electronic Components, IEEE, New York, pp.87–91, (1988).

[9] U.A. Jeigarnik, F.P. Ivanov and N.P. Ikranikov, "Experimental Data on Heat Transfer and Hydraulic Resistance in Unregulated Porous Structures," (in Russian), Teploenergetika, No.2, pp.33–38, (1991).

[10] G.J. Hwang and C.H. Chao, "Heat Transfer Measurement and Analysis for Sintered Porous Channels," *J. of Heat Transfer,* **116,** pp.456–464, (1994).

[11] K. Nasr, S. Ramadhyani and R. Viskanta, "An Experimental Investigation on Forced Convection Heat Transfer from a Cylinder Embedded in a Packed Bed," *ASME J. of Heat Transfer,* **116,** pp.73–80, (1994).

[12] C.Y. Choi and F.A. Kulacki, "Non-Darcian Effects on Mixed Convection in a Vertical Porous Annulus," Proc. 9th IHTC-Heat Transfer, **5,** pp.271–276, (1990).

[13] N.J. Kwendakwema and R.F. Boehm, "Parametric Study of Mixed Convection in Porous Medium between Vertical Concentric Cylinders," *ASME J. of Heat Transfer,* **113,** pp.128–134, (1991).

[14] B.X. Wang and J.H. Du, "Forced Convective Heat Transfer in Vertical Annuli Filled with Porous Media," *Int. J. Heat Mass Transfer,* **36,** pp.4207–4214, (1993).

[15] E. David, G. Lauriat and P. Cheng, "A Numerical Solution of Variable Porosity Effects on Natural Convection in a Packed-Sphere Cavity," *ASME J. of Heat Transfer,* **113,** pp.391–399, (1991).

[16] C.T. Hsu and P. Cheng, "Thermal Dispersion in a Porous Medium," *Int. J. Heat Mass Transfer,* **33,** No.8, pp.1587–1597, (1990).

[17] R. Clarksean, R. Golightly and R.F. Boehm, "An Experimental and Numerical Investigation of Mixed Convection in a Porous Medium between Vertical Concentric Cylinders," Proc. 9th IHTC-Heat Transfer 1990, Hemisphere, New York, **2,** pp.477–482, (1990).

[18] P.X. Jiang, B.X. Wang and Z.P. Ren, "A Numerical Investigation of Mixed Convection in a Vertical Porous Annulus," 10th Int. Heat Transfer Conference, Brighton, UK., **5,** pp.303–308, (1994).

[19] P.X. Jiang, B.X. Wang, D.A. Luo and Z.P. Ren, "Fluid Flow and Convective Heat Transfer in a Vertical Porous Annulus," Numerical Heat Transfer, Part A, **30,** No.3, pp.305–320, (1996).

[20] P.X. Jiang, Z.P. Ren, B.X. Wang and Z. Wang, "Forced Convective Heat Transfer in a Plate Channel Filled with Solid Particles," *J. of Thermal Science,* **5,** No.1, pp.43–53, (1996).

[21] E. Achenbach, "Heat and Flow Characteristics of Packed Beds," Experimental Thermal and Fluid Science, **10,** pp. 17–27, (1995).

[22] B.S. Petukhov, L.G. Genin and S.A. Kovalev, ≪Heat Transfer in Nuclear Power Equipment≫, (in Russian), Energoatomizdat Press, Moscow, (1986).

[23] V.V. Gnielinski, Forschung im Ingenieurwesen, Band. 41, Nr.1, s. 7–16, (1975).

[24] P. Cheng, C.T. Hsu and A. Chowdhury, "Forced Convection in the Entrance Region of a Packed Channel with Asymmetric Heating," *J. of Heat Transfer,* **110,** pp.946–954, (1988).

[25] P. Zehner and E.U. Schlunder, "Thermal Conductivity of Granular Materials at Moderate Temperature," (in German), Chemie Ingenieur Technik, **42,** pp.933–941, (1970).

[26] S.L. Rivkin and A.A. Aleksandrov, ≪Thermophysical Properties of Water and Steam≫, (in Russian), Moscow Energy Press, (1980).

[27] M.E. Aerov and O.M. Tojec, "Hydraulic and Thermal Basis on the Performance of Apparatus with Stationary and Boiling Granular Layer," (in Russian), Leningrad, Himia Press, (1968).